NUMERICAL PREDICTIONS OF ROTORCRAFT UNSTEADY AIR-LOADINGS AND BVI NOISE BY USING A TIME-MARCHING FREE-WAKE AND ACOUSTIC ANALOGY

Kihoon Chung and Changjeon Hwang
Rotor System Department, Korea Aerospace Research Institute, Daejeon, Republic of Korea

Youngmin Park
Aerodynamics Department, Korea Aerospace Research Institute, Daejeon, Republic of Korea

Wonju Jeon, Duckjoo Lee
Division of Aerospace Engineering, Korea Advanced Institute of Science and Technology, Daejeon, Republic of Korea

Abstract

The BVI (Blade Vortex Interaction) noise prediction has been one of the most challenging acoustic analyses in helicopter aeromechanical phenomenon. It is well known a high resolution airload data with accurate tip vortex positions are necessary for the accurate prediction of this phenomenon. The truly unsteady time-marching free-wake method, which is able to capture the tip vortices instability in hover and axial flights, is expanded with the rotor flapping motion and trim routine to predict an airloads in forward and descent flights. And the generalized Farassat formulation based on the FW-H equation is applied for noise prediction considering the blade flapping motion. At first, the time-marching free-wake method with trim routine is validated in AH-1G forward flight condition. The predicted airloads are quite well agreed with those of flight test. Then the descent flight condition of AH-1 OLS(Operational Load Survey) configuration is analyzed using newly developed prediction tools. The predicted sectional thrust distribution shows the present scheme is able to capture well the unsteady airload caused by a parallel BVI. And the predicted noise data at 3.4 times of rotor radius far from the hub center is quite good agreements with the experimental data compared to the other results.

Introduction

The BVI (Blade Vortex Interaction) phenomenon, especially parallel interactions between the helicopter main rotor blade and the tip vortex, is the cause of significant noise and vibration problems in helicopter operation. In particular, the descent and banked turn flight conditions are known to produce significant BVI. To predict a BVI noise accurately, the high resolution airloads data are prerequisite. And the better tip vortex position and strength predictions result in the more accurate BVI noise prediction.

This paper demonstrates the predicted aerodynamics and acoustics results of arbitrary rotor in forward flight. A time-marching free-wake method containing full rotor vortex system, which is coupled with trimming process, is used to predict the trim condition and unsteady airloads of AH-1G flight test [1] and small scaled AH-1 experiment in wind tunnel [2]. The BVI noise prediction of small scaled AH-1 is performed by using Farrasat 1-A method [3]. The major advantage of this scheme is its generality and fast computation. It models the trimming rotor blade motions, unsteady rotor wake system and the noise with a unified approach in short time by using parallel computations. It also can expand to include the helicopter fuselage and blade aeroelastic deformation.

However, the ultimate success of this method depends on the accurate prediction of the unsteady rotor wake. The wakes are genuinely unsteady even in hovering flight, which have been observed in various experiments [4-5]. The unsteady wake motion is becoming a crucial issue in the point of unsteady aerodynamics and aeroacoustics for a certain flight condition in recent years. The tip-vortex pairing phenomena of model AH-1G rotor are numerically predicted [7-8] and the computational results have quite good agreements with experimental wake pairing visualization data [6].

Historically, helicopter industries have used comprehensive helicopter analysis to model rotors in forward flight. These analyses contain phenomenological models for the blade aerodynamics and the wake. In these methods, the near wake is modeled as a vortex sheet across which the velocity potential is discontinuous. The effect of the far wake is typically computed from only tip vortex without inboard vortex or an external wake model [9-10]. But full inboard vortex is very important to capture the double tip vortexes at advancing side in fast forward and reversed flow condition at retreating side. During the early 1980s, computers became powerful enough to model helicopter aerodynamics using finite difference methods. Most current generation Euler or Navier-Stokes solvers are capable of capturing the rotor wake as a part of the solution [11-17]. Despite these advances, the blade loads prediction capability and the solution efficiency of the current generation of rotor CFD analyses are not at a level acceptable to the helicopter industry. The usefulness of these analyses is limited because the rotor is not trimmed, because the tip vortex capturing suffers from excessive numerical diffusion.

In this paper, at first the time marching free wake method is validated in forward flight condition, and then

demonstrates the capability of BVI noise prediction in descent flight condition.

Numerical Schemes

Unsteady Loading Prediction

The fluid surrounding the body is assumed to be inviscid, irrotational, and incompressible over the entire flow field, excluding the body's solid boundaries and its wakes. Therefore, a velocity potential $\Phi(\vec{x},t)$ can be defined and the continuity equation in the inertial frame becomes:

$$\nabla^2\Phi = 0 \tag{1}$$

The boundary condition requiring zero normal velocity across the body's solid boundaries is:

$$(\nabla\Phi + \vec{V}_{wake} - \vec{V})\cdot\vec{n} = 0 \tag{2}$$

where $\vec{V}_{wake}(\vec{x},t)$ is the induced velocity due to the vorticity field in the wake, $\vec{V}(\vec{x},t)$ is the body surface's velocity, and $\vec{n}(\vec{x},t)$ is the vector normal to the moving surface, as viewed from the blade.

Using Green's second identity, the general solution of Eq. (1) can be constructed by integrating the contribution of the basic solution of source (σ) and doublet (μ) distributions over the body's surface:

$$\Phi(\vec{x},t) = \frac{1}{4\pi}\int_{body+wake}\mu\vec{n}\cdot\nabla(\frac{1}{r})ds - \frac{1}{4\pi}\int_{body}\sigma(\frac{1}{r})ds \tag{3}$$

Inserting Eq. (3) into Eq. (2) becomes:

$$\{\frac{1}{4\pi}\int_{body+wake}\mu\nabla[\frac{\partial}{\partial n}(\frac{1}{r})]ds - \frac{1}{4\pi}\int_{body}\sigma\nabla(\frac{1}{r})ds - \vec{V}\}\cdot\vec{n} = 0 \tag{4}$$

The source term is neglected in the case of the thin blade. Thus, only the first part of Eq. (3) is used to represent the lifting surface. The constant-strength doublet panel is equivalent to a closed vortex lattice with the same strength of circulation, ($\Gamma = \mu$). Then the induced velocity of the vortex lattice in Eq. (4), representing the blade, can be obtained by using Biot-Savart's law:

$$\vec{V} = -\frac{1}{4\pi}\int_c\frac{\vec{r}\times\Gamma d\vec{l}}{|\vec{r}|^3} \tag{5}$$

The collocation point is at the mid-span and three-quarter chord of each. The boundary condition of no-flow penetration is satisfied at the collocation point of each lattice. The application of the flow tangency condition (Eq. 4) to the vortex lattice distribution yields the following linear matrix equation that is to be solved:

$$A_{ij}\Gamma_j = R_i \quad (i,j = 1,\cdots,n) \tag{6}$$

where A_{ij} is the coefficient matrix of normal induced velocity on the *i*-th element of the blade due to the *j*-th vortex lattice with the unit circulation, and Γ_j is the unknown circulation value of the blade vortex lattice. R_i is the normal induced velocity at each control point due to the free stream velocity, the blade-moving velocity, and the wake-induced velocity.

A three-dimensional wing trails the bound circulation (Γ) into the wake. Radial variation of bound circulation produces trailed vorticity in the wake, which direction is parallel to the local free stream direction at each instant it leaves the blade. Azimuthal variation of bound circulation produces shed vorticity, oriented radially in the wake. The strengths of the trailed and shed vorticities are determined by the radial and azimuthal derivatives of bound circulation at the instant the wake element leaves the blade. The bound circulation has a peak near the tip, and quickly drops to zero at the tip. The trailed sheet therefore has a high strength (proportional to the radial derivative of Γ) at the outer wake, and quickly rolls up into a concentrated tip vortex. The strength of the trailed shed wake vortex at this time step is set equal to the one of the vortex lattice elements, which is located at the trailing edge of the blade ($\Gamma_{T.E,t} = \Gamma_{wake,t}$). This condition is forced to satisfy the Kutta condition ($\gamma_{T.E} = 0$).

Since the wake surface is force-free, each vortex wake element moves with the local stream velocity, which is induced by the other wake element and the blade. The convection velocity of the wake is calculated in the inertial frame. The vortex wakes are generated at each time step. Therefore, the number of wake-elements increases as the blade is rotating. It is clear that a large number of line elements for the highly curved and distorted wake region like the tip vortex are necessary to describe the vortex filament distortions accurately. In general, computational time for the calculation of the wake distortion is proportional to the square of the vortex element number. Therefore, a curved element is used to reduce the number of elements.

There are many mathematical expressions to represent the three dimensional curves. Generally, cubic spline curves are used to describe the curves. However, the cubic spline curves have certain disadvantages; the cubic spline curves require a large tri-diagonal matrix inversion, and the numerical disturbance of position in any one segment affects all the global curve segments. Therefore, the curve is not adequate to represent the vortex filament motion in strong interaction problems. The parabolic blending curves, employed here, maintain the continuity of the first derivative in space, which is critical to self-induced vortex interactions and interactions with wake and blade. The parabolic blending curve, $C(\xi)$, is given

by

$$C(\xi) = (1-\xi)\,p(r) + \xi q(s) \tag{7}$$

The function of $p(r)$ and $q(s)$ are parametric parabolas through P_1, P_2, P_3 and P_2, P_3, P_4 as shown in Figure 1, respectively.

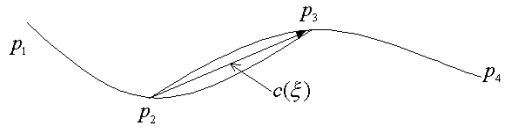

Figure 1. Parabolic blending method

A generalized parametric blending curve is developed from the assumption of normalized chord length approximation for the position parameters, r and s at P_2 and P_3 which are linearly related with the parameter ξ respectively, *i.e.* $0 \le r, s, \xi \le 1$. Then, this blending curve is applied to Eq. (5).

The induced velocity by a vortex filament with circulation is given by the usual cut-off approach, which is formulated by Moore-Rosenhead [12-13]. It is defined as

$$\vec{V} = \frac{1}{4\pi}\int_c \frac{\vec{r}}{(|\vec{r}|^2 + \mu^2)^{3/2}} \times \Gamma \frac{\partial y(\xi,t)}{\partial \xi} d\xi \tag{8}$$

Here, $y(\xi,t)$ is the position vector of a material point denoted by Lagrangian variable ξ at an instance, which describes a vortex filament with circulation Γ. The Rosenhead cut-off parameter μ is used to remove the singularity problem in the Biot-Savart's law at the region very closed to the vortex filaments. In this study, inboard shedding vortex elements as well as the trailed elements are kept for more rigorous representation of vortex dynamics and unsteadiness.

Blade Motion and Rotor Trim

Helicopter rotor in forward flight accompany periodic motion of the blade, which can be described by using the Fourier series as a function of azimuth angle, ψ:

$$\theta(\psi) = \theta_0 + \theta_{1c}\cos(\psi) + \theta_{1s}\sin(\psi) + \cdots \tag{9}$$
$$\beta(\psi) = \beta_0 + \beta_{1c}\cos(\psi) + \beta_{1s}\sin(\psi) + \cdots \tag{10}$$
$$\varsigma(\psi) = \varsigma_0 + \varsigma_{1c}\cos(\psi) + \varsigma_{1s}\sin(\psi) + \cdots \tag{11}$$

where θ, β, and ς represent the blade pitch, flap, and lead-lag angles, respectively. For a flap-lag-feather sequence, the usual rotational transformation sequence is flap followed by lag. For this case, the hub-fixed rotating axes xyz are related to the blade fixed axes $x_2 y_2 z_2$ according to

$$\begin{Bmatrix} x \\ y \\ z \end{Bmatrix} = [T_{FLT}] \begin{Bmatrix} x_2 \\ y_2 \\ z_2 \end{Bmatrix} \tag{12}$$

where

$$[T_{FLT}] = [T_\beta][T_\varsigma][T_\theta] = \begin{bmatrix} \cos\beta & 0 & -\sin\beta \\ 0 & 1 & 0 \\ \sin\beta & 0 & \cos\beta \end{bmatrix} \begin{bmatrix} \cos\varsigma & -\sin\varsigma & 0 \\ \sin\varsigma & \cos\varsigma & 0 \\ 0 & 0 & 1 \end{bmatrix} \begin{bmatrix} 1 & 0 & 0 \\ 0 & \cos\theta & -\sin\theta \\ 0 & \sin\theta & \cos\theta \end{bmatrix} \tag{13}$$

In order to match the calculated thrust to the desired level and to eliminate the rotor aerodynamic moments, a rotor trimming procedure is enforced in forward flight. The thrust and moment coefficients can be expressed as a function of collective and cyclic pitch angles.

$$\begin{aligned} C_T &= C_T(\theta_0, \theta_{1c}, \theta_{1s}) \\ C_{Mx} &= C_{Mx}(\theta_0, \theta_{1c}, \theta_{1s}) \\ C_{My} &= C_{My}(\theta_0, \theta_{1c}, \theta_{1s}) \end{aligned} \tag{14}$$

The estimated correction angles of the control settings, $\Delta\theta_0$, $\Delta\theta_c$ and $\Delta\theta_s$, can be obtained by using the Newton-Rhapson iterative methods.

$$\begin{pmatrix} \Delta\theta_0 \\ \Delta\theta_{1c} \\ \Delta\theta_{1s} \end{pmatrix} = \begin{pmatrix} \frac{\partial C_T}{\partial\theta_0} & \frac{\partial C_T}{\partial\theta_{1c}} & \frac{\partial C_T}{\partial\theta_{1s}} \\ \frac{\partial C_{Mx}}{\partial\theta_0} & \frac{\partial C_{Mx}}{\partial\theta_{1c}} & \frac{\partial C_{Mx}}{\partial\theta_{1s}} \\ \frac{\partial C_{My}}{\partial\theta_0} & \frac{\partial C_{My}}{\partial\theta_{1c}} & \frac{\partial C_{My}}{\partial\theta_{1s}} \end{pmatrix}^{-1} \times \begin{pmatrix} C_T{}^{desired} - C_T \\ -C_{Mx} \\ -C_{My} \end{pmatrix} \tag{15}$$

The trim solution requires some cycles before convergence. Each trim cycle consists of 12 rotations of the rotor, six for calculating the sensitivity and the rest for initial and final solution iteration.

Loading Noise Prediction

The Ffowcs Williams and Hawkings formulation, Eq. (16), has been successfully used for predicting rotor noise. The Ffowcs Williams and Hawkings formulation is expressed as follows;

$$\begin{aligned} 4\pi a_0{}^2 \overline{\rho}(x,t) &= \frac{\partial^2}{\partial x_i \partial x_j}\iiint \left[\frac{T_{ij}}{r|1-M_r|}\right] dV \\ &- \frac{\partial}{\partial x_i}\iint \left[\frac{P_{ij}n_j}{r|1-M_r|}\right] dS + \frac{\partial}{\partial t}\iint \left[\frac{\rho_0 v_n}{r|1-M_r|}\right] dS \end{aligned} \tag{16}$$

The terms inside a bracket are evaluated at a retarded time. The dipole term (the second term) and monopole term (the third term) can be expressed in a computationally convenient form from developed by Farassat [3] as shown in Eq. (17).

$$4\pi p'_L(x,t) = \frac{1}{a_0}\int_{f=0}\left[\frac{l_i\hat{r}_i}{r(1-M_r)^2}\right]dS + \int_{f=0}\left[\frac{l_r - l_i M_i}{r^2(1-M_r)^2}\right]dS + \frac{1}{a_0}\int_{f=0}\left[\frac{l_r(rM_i\hat{r}_i + a_0 M_r - a_0 M^2)}{r^2(1-M_r)^3}\right]dS \quad (17)$$

Here p'_L stands for the acoustic pressure due to loading. The dot on $M_i = v_i / a_0$ and l_i denote rate of variation of these vectors with respect to source time. Note that v_i is the local velocity of blade surface with respect to the frame fixed in the undisturbed medium.

Validation of Numerical Scheme

Prediction of Unsteady Tip-Vortex Geometry in Axial Flight

The rotor used in this wake calculation is AH-1G's 41-inch radius model rotating at 1800 rpm. The blade is modeled using 5 chordwise panels and 10 spanwise panels. This rotor is the same as that used in the experiments of Caradonna et al and Komerath et al [6]. Twenty-four time-steps are taken per blade revolution and the vortex core radius is taken as 10% of the chord length that is commonly used in rotor wake simulation. The tip-vortex pairing process has been quantified by using the trajectory tracking method.

The trajectories of the tip-vortices, which are calculated by using time-marching free-wake method, are shown in Figure 2. The left figure shows the three-dimensional view of tip vortex trajectories and the right one shows the cross section view of that.

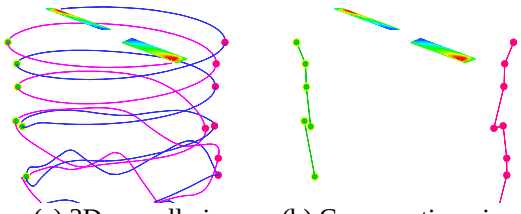

(a) 3D overall view (b) Cross section view

Figure 2. 3-D view and cross section view of wake geometries at 11^o collective angle, 9.6 fps climb rate

Figure 3 shows the tip-vortices trajectories for collective angle of 11^o at the climb rate of 9.6 fps. These trajectories clearly show that the local radial expansion is the result of adjacent tip vortices beginning to pair together and spiral about each other. The computed wake geometries show excellent agreements with the experimental data as the higher collective angle.

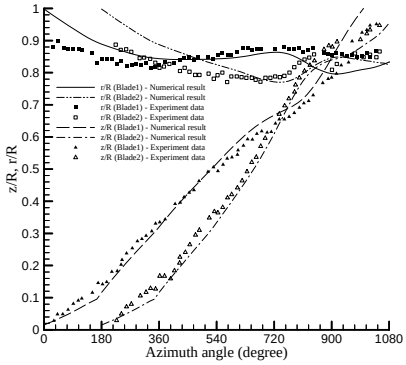

Figure 3. Wake geometries at 11^o collective angle, 9.6 fps climb rate

Prediction of Airloads in Forward Flight

To validate the numerical scheme in forward flight condition, the forward flight of two-bladed teetering rotor of AH-1G is simulated. The blade has a rectangular planform with a symmetric airfoil. The aspect ratio of the blade is 9.8 and the linear twist rate is -10 deg from root to tip. The calculated flight condition at which the flight test data is available corresponds to an advance ratio of 0.19, tip Mach number of 0.65, and a time-averaged total thrust coefficient of 0.00464 [15]. This particular flight condition has also studied by Ahmad and Duque [16] and Yang et al. [17].

Table 1. Control and flapping angles of AH-1G rotor

Blade Motion	θ_0	θ_{1s}	θ_{1c}	β_{1s}	β_{1c}
Flight Test [Ref. 15]	6.0	-5.5	1.7	-0.15	2.13
Yang et al., after trim	8.0	-6.5	2.5	-0.15	2.13
Present Prediction, after trim	6.1	-5.6	1.4	-0.15	2.13

In the present prediction, the collective pitch is adjusted to match the measured overall thrust. To eliminate the rolling and pitching moment, the lateral and longitudinal cyclic pitch angles were also trimmed automatically. The trimmed first blade harmonics (in degrees) are given in Table 1. In Table 1, the predicted trim condition shows good agreements with those of flight test although a fuselage, hub, and blade elastic deformation effects are not considered.

Figure 4 compares the present computed normal load data with the measured airloads [15] and previous studies [16-17]. The present predicted results agree very well with flight test data. Therefore, the present numerical scheme, i.e. time-marching free wake method with trim routine is working very well even in forward flight condition.

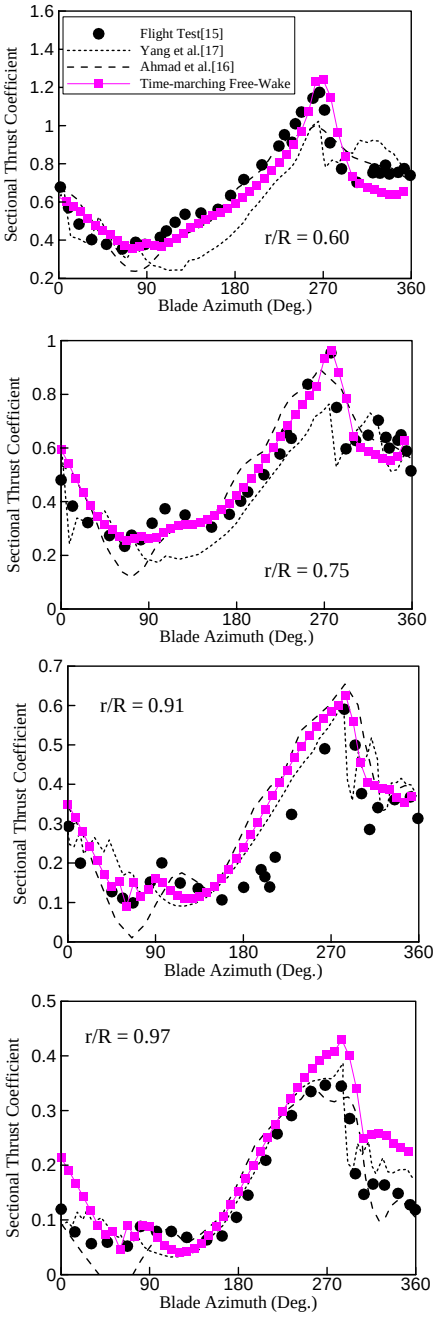

Figure 4. Sectional thrust coefficient comparisons for AH-1G rotor

Prediction of Inflow in Forward Flight

To validate the time averaged inflow prediction capability of the present method, the same experiment condition as Elliott et al.[18] is simulated. The experimental data were measured one chord above the rotor disk by using a laser Doppler velocimetry system. The rotor was trimmed such that the TPP(Tip Path Plane) was perpendicular to the rotor shaft, with a forward shaft tilt of -3 degrees. The conditions of the simulation are $C_T = 0.008$, $\alpha_s = -3^o$ and $\mu = 0.15$.

Figure 5 shows the comparisons of inflow ratio between those of Drees linear inflow model [9], the experimental data [18], Mangler & Squire model [9], and the predicted result that is simulated by using the present scheme. In case of Mangler & Squire model, the average value of Type I and Type III is used as recommended in Ref. 9. Because the model of experiment is not employed with an isolated rotor but a rotor with fuselage, the calculated results cannot be considered in entire attributes of experimental data.

The predicted result shows reasonably good agreements with the experimental data. In Fig. 5(a), some discrepancies of longitudinal inflow near the leading edge region of the rotor disk (negative x/R in Fig. 5 (a)) may be caused by upwash due to a fuselage effect. Lateral inflow is predicted with better agreement as shown in Fig. 5(b).

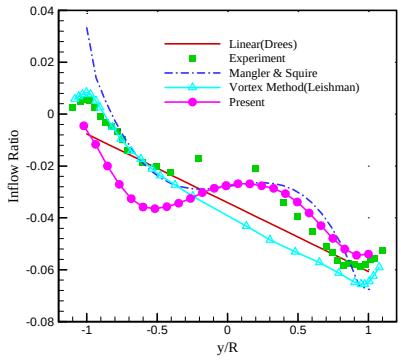

(a) Longitudinal inflow

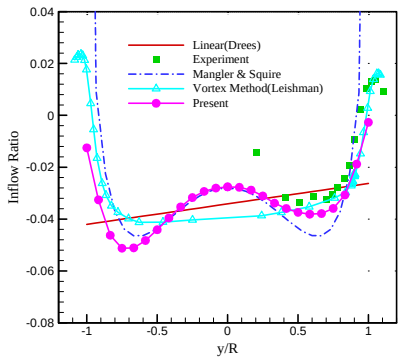

(b) Lateral inflow

Figure 5. Comparisons of inflow ratio across the disk in forward flight($\mu = 0.15$)

Results

The rotor used in this BVI noise prediction is a 1/7 scale model of AH-1 helicopter main rotor [20]. These rotor blades are rectangular with 8.2^o of twist from root to tip and have a precone angle of 0.5^o. The rotor has a radius, R, equal to 9.22 chord lengths with a blade root cut at 0.182R. The aerodynamic conditions are set to a hover-tip Mach number of 0.664, an advance ratio of 0.164, and a thrust coefficient of 0.0054. The shaft angle is 0^o, however the rotor tip-path plan is tilted back by

1^o using longitudinal flap control.

Numerical simulation for a forward flight requires the complete blade motions. Table 2 shows trimmed first blade harmonics (in degrees).

Table 2. Control and flapping angles of AH-1 1/7 scale model rotor for BVI condition

Blade Motion	θ_0	θ_{1s}	θ_{1c}	β_0	β_{1s}	β_{1c}
Experiment [Ref. 20]	6.14	-1.39	0.9	0.5	0.0	-1.0
Present Prediction, after trim	6.07	-2.37	1.2	0.5	0.0	-1.0

The blade is modeled using 12 chordwise panels and 40 spanwise panels. 180 time-steps are taken per blade revolution and the vortex core radius is taken as 10% of the chord length that is commonly used in rotor wake simulation.

Figure 6 shows the geometries of the rotor and the trailed wakes computed by time-marching free-wake method. Form figure 6, It can be check again that some trailed wakes located outboard rotate with each others and form tip-vortex and this tip-vortex interact with blade. Due to this BVI, the air loading of a blade varies versus azimuthal rotation as shown in figure 7.

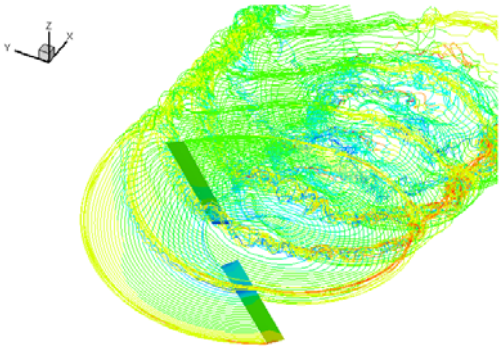

Figure 6. Computed rotor and wake geometries

Figure 7 shows the BVI location on the rotor disk. Figure 7 (a) is the sectional thrust coefficient of present freewake result and figure 7 (b) is the BVI locations of previous research [21]. In the top-view, BVI location calculated by present method is almost same with previous research results as shown in figure 7.

The predicted blade loads at several spanwise locations are shown in figure 8. From these plots, a few points can be observed. First, present free-wake predicts lower between 270 degree and 90 degree and predicts intermediate value between 90 degree and 270 degree. Secondly, the present free-wake and DLR code predict multiple interactions, while the other two codes predict a single strong interaction. Thirdly, predicted occurrence of interaction peakes by present free-wake are located between AFDD and DLR.

(a) Sectional thrust distribution (present freewake)

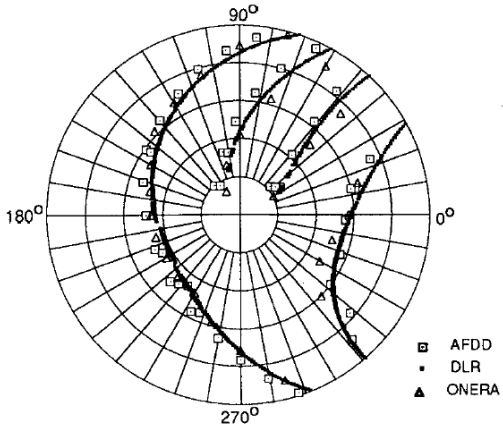

(b) BVI trajectories of previous researches [21]

Figure 7. BVI location on the rotor disk (top view)

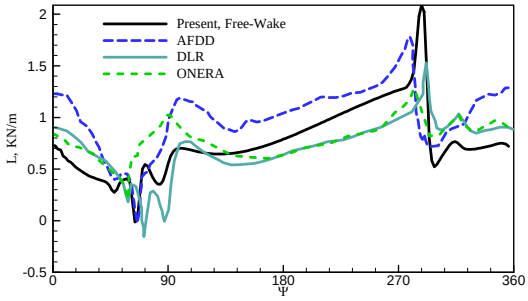

(a) OLS local blade loading (r/R=0.91)

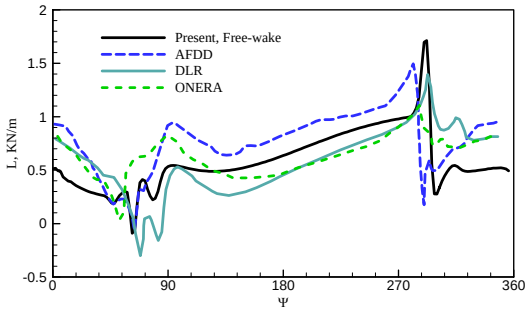

(c) OLS local blade loading (r/R=0.955)

Figure 8. Comparisons of predicted results for BVI air loadings (AFDD, DLR, ONERA data from [21])

Figure 9 shows the time history of thrust coefficient. After 2 revolutions, thrust coefficient goes to periodic state. Therefore, air loadings after 2 revolutions are used to calculate the BVI loading noise as input to acoustic solver.

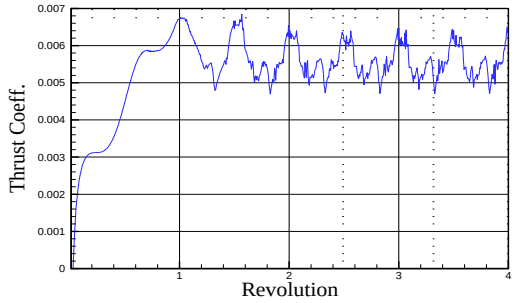

Figure 9. Time history of thrust coefficient

Noise signals are calculated at the location that is apart from rotor as 1.72D, longitudinally $\varphi = 30^o$ below the rotor plane, and laterally $\psi = 180^o$. Figure 10 shows the BVI noise signals in time domain of various predicted results and experiment. Figure 10 (a), (b), and (c) show the noise signals predicted by the present method, AFDD [21] and Roger C. Strawn et al's CFD [22] results. The noise signal predicted by the present free-wake can capture the higher first and second peaks than those by AFDD and is more similar to experiment data. But the present free-wake can't capture well the peak drop near blade azimuth 70 degree as like Roger C. Strawn et al's CFD result.

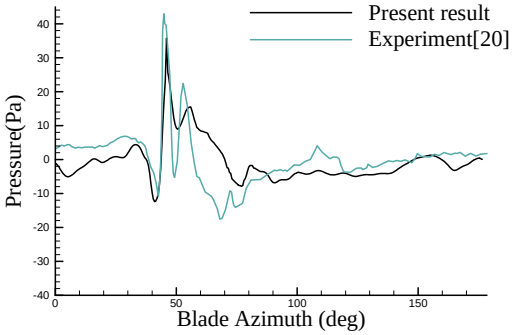

(a) Present result vs. experimental data [20]

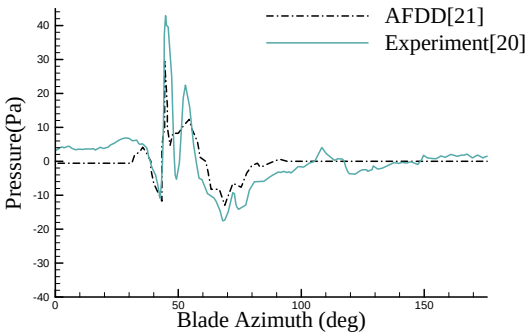

(b) AFDD result [21] vs. experimental data [20]

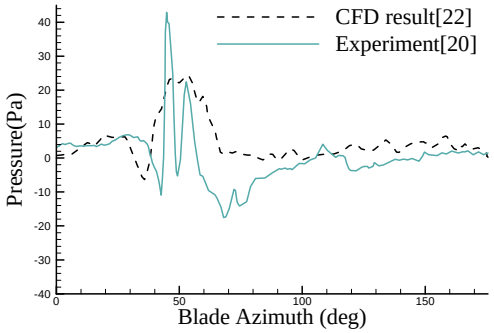

(c) CFD result [22] vs. experimental data [20]

Figure 10. Comparisons of BVI noise time histories.

Conclusion

In this study, the truly unsteady time-marching free-wake method, which is able to capture the tip vortices instability in hover and axial flights, is expanded with the rotor flapping motion and trim routine to predict airloads in forward and descent flights. And the generalized Farassat formulation based on the FW-H equation is applied for noise prediction considering the blade flapping motion. At first, the time-marching free- wake method with trim routine is validated in AH-1G forward flight condition. Then the descent flight condition of AH-1 OLS(Operational Load Survey) configuration is analyzed using newly developed prediction tools.

The following conclusions have been drawn from this study:

1. The time-marching free-wake method with trim routine is able to predict the forward flight air-load quite accurately.

2. The comparisons of time averaged inflow distribution show the present scheme is able to predict the inflow well especially in the main lifting region (50%R~85%R) than the other vortex method.

3. The predicted sectional thrust distribution in descent flight condition of AH-1 OLS configuration shows the present scheme is able to capture well the unsteady air-load caused by a parallel BVI with moderate sizes of chordwise, radial and azimuthal steps.

4. The predicted noise data at 3.4 times of rotor radius far from the hub center is quite good agreements with the experimental data compared to the other results in terms of primary and secondary peak pressures.

Acknowlegdement

This study was a part of results of the project entitled in "Innovative Technology Study for the Jet-Smooth Quiet Rotor System" supported by the Korea Research Council of Public Science and Technology..

References

1. Cross, J. L., and Watts, M. E., “Tip Aerodynamics and Acoustics Test:A Report and Data Survey,” NASA-RP-1179, NASA Ames Research Center, Dec. 1988.
2. Boxwell, D. A., Schmitz, F. H., Splettstoesser,W. R. and Schultz, K. J., “Helicopter Model Rotor-Blade Vortex Interaction Impulsive Noise: Scalability and Parametric Variations,” *Journal of American Helicopter Society*, Vol. 32, No. 1, Jan. 1987, pp. 3–12.
3. Farassat, F., "The Evolution of Methods for Noise Prediction of High Speed Rotor and Propellers in Time Domain," *Proceedings of an International Symposium held at Stanford University*, August 22-26, 1983, pp.129-147.
4. Landgrebe, A. J., "The Wake Geometry of a Hovering Helicopter Rotor and Its Influence on Rotor Performance," J. American Helicopter Soc., 17, (4), Oct., 1972, pp. 3-15.
5. Tangler, J. L., Wohlfed, R. M., and Miley, S. J., “An Experimental Investigation of Vortex Stability, Tip Shapes, Compressibility, and Noise for Hovering Model Rotor,” NASA CR-2305, 1973.
6. Caradonna, F., Hendley, E., Silva, M., Huang, S., Komerath, N., Reddy, U., Mahalingam, R., Funk, R., Ames R., Darden, L., Villareal, L., Gregory, and Wong, O., "An Experimental Study of a Rotor In Axial Flight," AHS Specialists' Meeting on Aerodynamics and Aeroacoustics, Williamsburg, VA, Oct. 1997.
7. Ki-Hoon Chung, Seon-Uk Na, Wanho Jeon and Duck-Joo Lee, "A Study on Rotor Tip Vortex Pairing Phenomenon by Using a Time-Marchig-Free-Wake Method", American Helicopter Society 56th Annual Forum, Virginia Beach, May 2-4, 2000.
8. K.H.Chung and D.J.Lee, " Numerical Prediction of Rotor Tip Vortex Roll-up in Climb Flight by Using a Time-Marchig-Free-Wake Method," Computational Fluid Dynamics Journal, pp. 80~88, vol. 12, no.1, April, 2003.
9. Johnson, W., “Development of a Comprehensive Analysis for Rotorcraft, I. Rotor Model and Wake Analysis,” *Vertica*, Vol. 5, No. 2, 1981, pp. 90–130.
10. Johnson, W., “Development of a Comprehensive Analysis for Rotorcraft, II. Aircraft Model, Solution Procedure and Applications,” *Vertica*, Vol. 5, No. 3, 1981, pp. 185–216.
11. Sankar, L. N., and Tung, C., “Euler Calculations for Rotor Configurations in Unsteady Forward Flight,” *Proceedings of the 42nd Annual Forum of the American Helicopter Society*, AHS International, Alexandria, VA, 1986.
12. Srinivasan, G. R., and Baeder, J. D., “TURNS: A Free Wake Euler/Navier–Stokes Numerical Method for Helicopter Rotors,” *AIAA Journal*, Vol. 31, No. 5, 1993, pp. 959–962.
13. Hariharan, N., “High Order Simulation of Unsteady Compressible Flows over Interacting Bodies with Overset Grids,” Ph.D. Dissertation, Aerospace Engineering, Georgia Inst. of Technology, Atlanta, GA, Aug. 1995.
14. Bangalore, A., and Sankar, L. N., “Forward Flight Analysis of Slatted Rotors Using Navier–Stokes Methods,” AIAA Paper 96-0675, Jan. 1996.
15. Ahmad, J., and Duque, E. P. N., “Helicopter Rotor Blade Computation in Unsteady Flows Using Moving Embedded Grids,” AIAA Paper 94-1922, June 1994.
16. Bauchau, O. A., and Ahmad, J. U., “Advanced CFD and CSD Methods for Multidisciplinary Applications in Rotorcraft Problems,” *Proceedings of the AIAA/NASA/USAF Multidisciplinary Analysis and Optimization Symposium*, AIAA, Reston, VA, 1996, pp. 945–953.
17. Sankar, L. N., Bharadvaj, B. K., and Tsung, F.-L., “Three-Dimensional Navier–Stokes/Full Potential Coupled Analysis for Transonic Viscous Flow,” *AIAA Journal*, Vol. 31, No. 10, 1993, pp. 1857–1862.
18. Elliot, J. W., Althoff, S. L., and Sailey, R. H., “Inflow Measurements Made with a Laser Velocimeter on a Helicopter Model in Forward Flight,” Vol. II and Vol. III, NASA TM-100542, TM-100543, 1988
19. Yang, Z., Sankar, L. N., Smith, M. J., Bauchau O.,”Recent Improvements to a Hybrid Method for Rotors in Forward Flight,” *Journal of Aircraft*, Vol. 39, No. 5, September-October, 2002.
20. Splettstoesser, W. R., Schultz, K. J., Boxwell, D. A., and Schmitz, F. H., “Helicopter Model Rotor-Blade Vortex Interaction Impulsive Noise: Scalability and Parametric Variations” presented at the 10th European Rotorcraft Forum, The Hague, Netherlands, Aug. 28-31, 1984.
21. Yu, Y. H., Tung, C., Gallman, J., Schultz, K. J., van der Wall, B., Speigel, P., and Michea, B., “Aerodynamics and Acoustics or Rotor Blade-Interaction,: AIAA Journal of Aircraft, Vol. 32, No. 5, Sept.-Oct., 1995, pp. 970-977.
22. Roger C. Strrwan, Jasim Ahmad and Earl P.N. Duque, “Rotorcraft Aeroacoustic Computations with Overset-Grid CFD Methods”, Presented at the AHS 54th Annual Forum, Washington, DC, May 22-24, 1998.